

## TEM Study of Electrochemical Cycling-Induced Damage and Disorder in LiCoO<sub>2</sub> Cathodes for Rechargeable Lithium Batteries

Haifeng Wang, Young-II Jang,\* Biying Huang,\* Donald R. Sadoway,\* and Yet-Ming Chiang\*

Department of Materials Science and Engineering, Massachusetts Institute of Technology, Cambridge, Massachusetts 02139, USA

Among lithium transition metal oxides used as intercalation electrodes for rechargeable lithium batteries, LiCoO<sub>2</sub> is considered to be the most stable in the  $\alpha$ -NaFeO<sub>2</sub> structure type. It has previously been believed that cation ordering is unaffected by repeated electrochemical removal and insertion. We have conducted direct observations, at the particle scale, of damage and cation disorder induced in LiCoO<sub>2</sub> cathodes by electrochemical cycling. Using transmission electron microscopy imaging and electron diffraction, it was found that (i) individual LiCoO<sub>2</sub> particles in a cathode cycled from 2.5 to 4.35 V against a Li anode are subject to widely varying degrees of damage; (ii) cycling induces severe strain, high defect densities, and occasional fracture of particles; and (iii) severely strained particles exhibit two types of cation disorder, defects on octahedral site layers (including cation substitutions and vacancies) as well as a partial transformation to spinel tetrahedral site ordering. The damage and cation disorder are localized and have not been detected by conventional bulk characterization techniques such as X-ray or neutron diffraction. Cumulative damage of this nature may be responsible for property degradation during overcharging or in long-term cycling of LiCoO<sub>2</sub>-based rechargeable lithium batteries. © 1999 The Electrochemical Society. S0013-4651(98)05-079-4. All rights reserved.

Manuscript submitted May 27, 1998; revised manuscript received September 15, 1998.

Lithium cobalt oxide, presently the most widely used cathode (positive electrode) intercalation compound in lithium-ion rechargeable batteries, is considered to be highly stable in the  $\alpha$ -NaFeO<sub>2</sub> structure type. LiCoO<sub>2</sub> synthesized by firing at high temperatures, often referred to as "HT-LiCoO<sub>2</sub>", has a highly ordered cation sublattice in which Li and Co ions occupy alternating {111} layers of octahedral sites in a nearly cubic close-packed oxygen sublattice.<sup>1-4</sup> The structure is rhombohedral (R3m space group) with lattice parameters  $a = 2.816 \text{ \AA}$  and  $c = 14.051 \text{ \AA}$  in the hexagonal setting.<sup>1,3</sup> LiCoO<sub>2</sub> processed at low temperatures (e.g., 400°C) often exhibits cation disorder,<sup>5-10</sup> and has come to be known as "LT-LiCoO<sub>2</sub>" despite the fact that processes have been discovered by which a high degree of  $\alpha$ -NaFeO<sub>2</sub> ordering can be obtained at low temperatures. For example, Amatucci et al.<sup>11</sup> used a hydrothermal method to obtain HT-LiCoO<sub>2</sub> from cobalt hydroxide, while Chiang et al.<sup>12</sup> used a solid-state intercalation reaction of lithium hydroxide with cobalt hydroxide to obtain HT-LiCoO<sub>2</sub>, in both instances at temperatures well below 400°C. Although some uncertainty remains regarding the structure of LT-LiCoO<sub>2</sub>, as discussed later, there is little doubt that the equilibrium structure of fully lithiated LiCoO<sub>2</sub> is the  $\alpha$ -NaFeO<sub>2</sub> polymorph.

The excellent electrochemical stability of HT-LiCoO<sub>2</sub> upon extended cycling<sup>5,6,13,14</sup> has been attributed largely to its structural stability, wherein the layered cation ordering is preserved upon repeated insertion and removal of Li<sup>+</sup>. During delithiation, Li<sub>x</sub>CoO<sub>2</sub> undergoes a sequence of phase transformations involving Li ordering within its octahedral layers, accompanied by changes in crystal symmetry, first to the monoclinic and then to the hexagonal phase.<sup>13-15</sup> Nonetheless, throughout this process it has been believed that Li and Co remain in their respective octahedral site layers. In situ X-ray diffraction of electrochemically cycled Li<sub>x</sub>CoO<sub>2</sub><sup>14</sup> indicates that as  $x \rightarrow 0$ , the layers of CoO<sub>6</sub> octahedral which initially have a CdCl<sub>2</sub> type of stacking sequence translate with respect to one another, forming hexagonal CoO<sub>2</sub> with the stacking sequence of CdI<sub>2</sub>. However, even this pure end-member can apparently be fully reintercalated to obtain HT-LiCoO<sub>2</sub> that subsequently has good cycling characteristics. The fact that the typical reversible limit of delithiation for Li<sub>x</sub>CoO<sub>2</sub> in commercial batteries is  $x \sim 0.5$ ,<sup>2,16</sup> corresponding to a charge capacity of  $\sim 140 \text{ mAh/g}$ , has been mostly attributed to mechanical failure associated with the large change in  $c$  axis dimension, rather than any changes in cation ordering. A recent study used acoustic emission to detect fracture events taking place upon electrochemical cycling.<sup>17</sup>

In the present work we have used transmission electron microscopy (TEM) to study microstructural damage, including features such as lattice strain, extended defects, and microfractures, as well

as changes in cation ordering resulting from electrochemical cycling. The results reveal effects that are not detectable through bulk analytical methods such as X-ray and neutron diffraction.

### Experimental

LiCoO<sub>2</sub> powder was synthesized by firing hydroxide precursors prepared according to Ref. 12 at 800°C for 2 h in air. An excess of the Li salt yielding an overall Li:Co molar ratio of 1.05:1 was used to compensate for possible Li loss during firing. Both XRD and single-crystal selected-area diffraction (SAD) showed that the starting material was well ordered in the  $\alpha$ -NaFeO<sub>2</sub> structure type. This powder was thoroughly tested in a separate study<sup>18</sup> and exhibited excellent electrochemical properties. Figure 1a shows the X-ray powder diffractogram for the starting powders, and Fig. 1b shows a representative SAD pattern taken of a single-crystal particle with the electron-beam along the [0001] zone axis.

The preparation of the cathodes and the testing procedures are discussed in detail in Ref. 18. Briefly, cathodes were prepared by mixing the as-calcined LiCoO<sub>2</sub> powder with carbon black (Cabot), graphite (TIMCAL America) and poly(vinylidene fluoride) (PVDF) (Aldrich) in a weight ratio of 78:6:6:10. The test cells consisted of two stainless steel electrodes with a Teflon holder. Lithium ribbon of 0.75 mm thickness (Aldrich) was used as the anode, Celgard 2400<sup>TM</sup> (Hoechst-Celanese, Charlotte, NC) as the separator, and a 1 M solution of LiPF<sub>6</sub> in ethylene carbonate (EC) and diethylene carbonate (DEC) (EC:DEC = 1:1 by volume) as the electrolyte. The charge-discharge studies were performed with a MACCOR automated tester (series 4000). We focused in particular on a cell that was electrochemically cycled 50 times between 2.5 and 4.35 V at charging and discharging current densities of 0.4 mA/cm<sup>2</sup> (C/5 rate), and terminated in the discharged state at 2.5 V. The first and 50th charge-discharge curves are shown in Fig. 2a, and the specific capacity vs. cycle number is shown in Fig. 2b. It is seen that after some initial fade, the discharge capacity is maintained at approximately 130 mAh/g out to 50 cycles.

The cell was then disassembled and the cathode was examined by X-ray diffraction directly after removal from the cell. Pieces of the cathode were ultrasonically de-agglomerated and dispersed on an amorphous carbon film supported by a Cu grid for TEM observation. A JEOL-2000FX TEM (JEOL USA Inc., Peabody, MA) operating at 200 kV accelerating voltage and equipped with a double-tilt holder was used for imaging and electron diffraction. All bright-field imaging was recorded using the central transmitted beam only, so that the contrast of microstructural features in different samples could be compared. The electron diffraction patterns were indexed in comparison with model crystal structures as discussed below.

\* Electrochemical Society Active Member.

### Structure Modeling

A large number of possible derivatives of the ideal HT-LiCoO<sub>2</sub> and spinel LiCo<sub>2</sub>O<sub>4</sub> structures were considered. The single-crystal SAD pattern as well as the corresponding powder XRD pattern for each was computed using the commercial software Cerius<sup>2</sup> (Version 3.5, Molecular Simulations, Inc., San Diego, CA). The same instrumental conditions were input into the simulation as used in the actual experiments. The lattice parameter is a fixed input parameter in these simulations. Stoichiometric model structures (overall composition LiCoO<sub>2</sub> or Li<sub>2</sub>Co<sub>2</sub>O<sub>4</sub>) are listed in Table I according to the space group and cation distribution. Nonstoichiometric structures were also modeled, as discussed later. In the modeled crystals, cation disorder (mixing and nonstoichiometry) was introduced using two approaches. The first creates a "mixed element" with hypothetical properties that are the weighted averages of the properties of the constituent atoms (e.g., element M = 75% Li + 25% Co). The properties averaged include the mass, van der Waals radius, covalent radius, metallic radius, ionicity, and atomic scattering factor. As a result, all disordered lattice sites have an identical chemistry and site

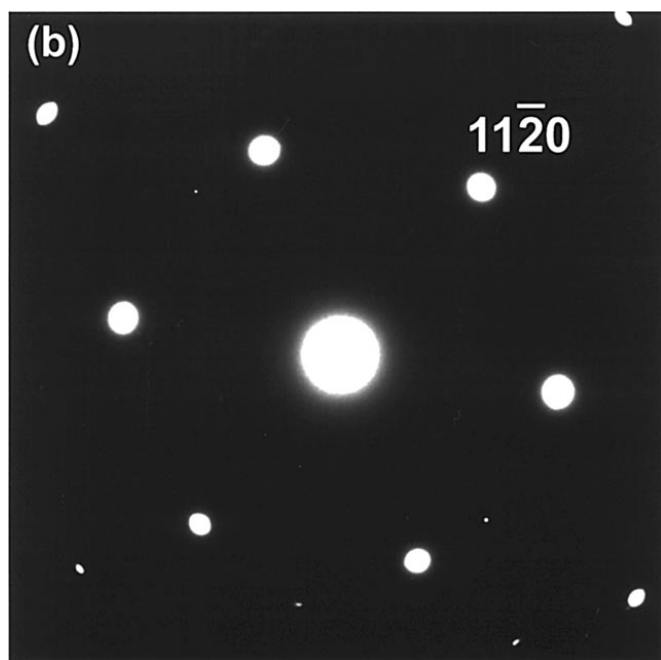
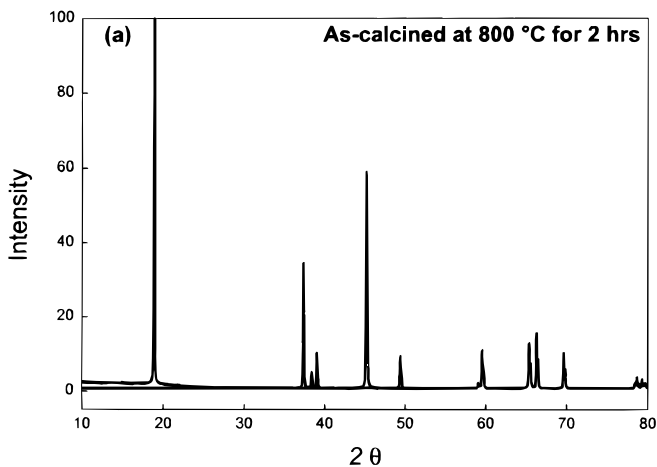


**Figure 1.** Experimental (a) X-ray diffractogram and (b) single-crystal selected-area diffraction pattern ([0001] projection) for as-fired LiCoO<sub>2</sub> powder.

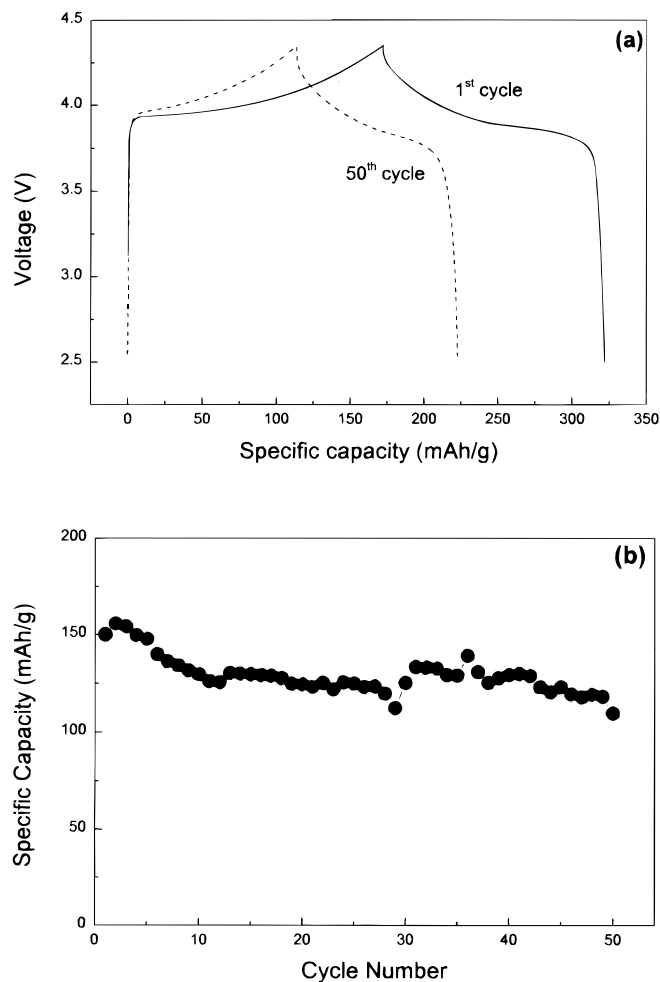


**Figure 2.** (a) Charge-discharge curve at the first and 50th cycle, and (b) specific capacity vs. cycle number, for present materials cycled between 2.5 and 4.35 V at 0.4 mA/cm<sup>2</sup> (C/5 rate).

symmetry. This approach is appropriate for simulating powder X-ray diffraction patterns for a disordered crystal with no superstructure.

The second approach introduces a substitutional disorder or nonstoichiometry by replacing one atom with another (including vacancies) randomly into the modeled cell at a specific concentration. This approach is ideal for simulating the single-crystal SAD patterns resulting from a particular type of disorder. For an infinitely large unit cell, the powder XRD pattern obtained by this approach would be identical to that by the "mixed element" method provided that there is no symmetry change. However, because the unit cells for modeling substitutional disorder are always limited and were eight unit cells in size in the present case, in order to limit the computing time, it was not possible to model substitutions without introducing long-range periodicity. This gives rise to superstructure reflections that are an artifact of the model and which were not seen experimentally. We ignored these and instead focused on the new reflections that were seen experimentally. These are reflections for which the structure factor<sup>19</sup> is zero in the perfect structure, i.e., are forbidden reflections. The presence of these reflections reflects a nonzero structure factor. We used the model simulations to understand the origin of these reflections, and also computed their structure factor separately in order to show that they result from cation disorder and are not an artifact of the modeling.

### Results and Discussion

**Cycling-induced microstructural damage.**—The as-fired LiCoO<sub>2</sub> powders were aggregated due to sintering and consisted of equiaxed particles ranging in size from 300 to 500 nm, as shown in Fig. 3a.

**Table I. Modeled structures for LiCoO<sub>2</sub> in R $\bar{3}$ m and Fd $\bar{3}$ m space groups with varying symmetry and octahedral/tetrahedral site occupancy.**

No.	Name	Space group	Cation position and occupancy
1. Varying octahedral site occupancy			
1	Ordered HT-LiCoO <sub>2</sub>	R $\bar{3}$ m	3a site: 100% Co 3b site: 100% Li
2	Partially disordered HT-LiCoO <sub>2</sub>	R $\bar{3}$ m	3a site: 75% Co + 25% Li 3b site: 75% Li + 25% Co
3	Fully disordered HT-LiCoO <sub>2</sub>	R $\bar{3}$ m	3a site: 50% Co + 50% Li 3b site: 50% Li + 50% Co
4	Cubic Li <sub>2</sub> Co <sub>2</sub> O <sub>4</sub> ("lithiated spinel")	Fd $\bar{3}$ m	16c site: 100% Li 16d site: 100% Co
5	Partially disordered Li <sub>2</sub> Co <sub>2</sub> O <sub>4</sub>	Fd $\bar{3}$ m	16c site: 75% Li + 25% Co 16d site: 75% Co + 25% Li
6	Fully disordered Li <sub>2</sub> Co <sub>2</sub> O <sub>4</sub>	Fd $\bar{3}$ m	16c site: 50% Li + 50% Co 16d site: 50% Co + 50% Li
2. Varying tetrahedral occupancy			
7	Li <sub>2</sub> Co <sub>2</sub> O <sub>4</sub> spinel with partial 8a tetrahedral site occupancy	Fd $\bar{3}$ m	8a site: 50% Li 16c site: 75% Li 16d site: 100% Co
8	Li <sub>2</sub> Co <sub>2</sub> O <sub>4</sub> spinel with full 8a tetrahedral site occupancy	Fd $\bar{3}$ m	8a site: 100% Li 16c site: 50% Li 16d site: 100% Co
9	LiCoO <sub>2</sub> , normal spinel structure	Fd $\bar{3}$ m	8a site: 100% Li 16d site: 100% Co
10	Li <sub>2</sub> Co <sub>2</sub> O <sub>4</sub> spinel, randomized tetrahedral site occupancy	Fd $\bar{3}$ m	All equivalent tetrahedral sites: 25% Li 16d site: 100% Co

Little variation in contrast across individual particles is seen except for that due to thickness variation, consistent with a high level of crystalline perfection, and the electron diffraction results (Fig. 1b) showing a single, well-ordered  $\alpha$ -NaFeO<sub>2</sub> phase in the starting material.

A bright-field image of the composite cathode is shown in Fig. 4, in which a LiCoO<sub>2</sub> particle, the carbon black, and graphite are identified. After electrochemical cycling the oxide powder particles show new features in bright-field imaging that are due to diffraction contrast (Fig. 3b). Some particles appear to be relatively unchanged, whereas others show a variety of contrast features including strain contours, dislocations and other extended defects, and microcracks (Fig. 3b and 5). Approximately 50% of the particles showed some sign of damage, with differing extents of lattice strain, whereas the remainder exhibited contrast very similar to the as-fired particles. Approximately 20% of the particles examined were fractured. Figure 5 shows individual highly strained particles in which microcracks are clearly visible (indicated by arrows). It was also observed that fractured particles sometimes contained an unstrained region apparently relieved of stress by the fracture event (Fig. 5b).

The wide variation in damage between particles indicates that not all LiCoO<sub>2</sub> particles in a composite cathode are charged and discharged equally during the electrochemical cycling. The cation disorder discussed later also supports the existence of locally varying levels of charge/discharge. This can be attributed to variations in electronic and ionic transport to individual particles, which are to be expected in a randomly mixed multiphase composite.

Considered in detail, several possible mechanisms can cause the strain damage. First, stresses can arise from lattice expansion and contraction, because upon delithiation, Li<sub>x</sub>CoO<sub>2</sub> exhibits a *c* axis expansion of up to 1.8% at  $x \cong 0.5$ , followed by a *c* axis contraction of up to -1.8% at  $x \cong 0.2$ .<sup>14</sup> A slight *a* axis contraction is observed up to  $x = 0.5$ , which is recovered upon further Li removal until the transformation to the monoclinic phase occurs.<sup>14</sup> The lattice strain is therefore both anisotropic and directly correlated with lithium concentration. However, uniform expansion or contraction of an unstrained particle should not result in the kind of damage seen here; differential lattice strain is necessary. We assume that LiCoO<sub>2</sub>, like most oxides, can tolerate elastic strain of ~0.1% before fracture. Therefore, one likely mechanism is that individual particles in a sintered polycrystalline aggregate are physically constrained by their neighboring particles, and stresses arise due to the anisotropic expansion and contraction that accompanies cycling. This mechanism is exactly analogous to the thermal stresses that arise from temperature cycling of materials with anisotropic thermal expansion coefficients. A second possible damage mechanism is differential expansion within a single particle, due to Li concentration gradients generated during charging and discharging. A third possible mechanism is the irreversible formation of extended defects when the Li concentration is overly depleted locally, resulting in phase transformation.<sup>13-15</sup> These transformations have been studied only by bulk X-ray diffraction, so it is not known whether or not they introduce crystallographic defects. Of these three mechanisms, the first can be considered to be definitely active, because the powders are clearly in the form of sintered aggregates. The relative importance of the other mechanisms cannot be established at this time.

*Cycling-induced cation disorder.*—Comparing the X-ray diffraction patterns of as-calcined (Fig. 1a) and cycled cathodes (Fig. 6), we note that the characteristic peak positions of the LiCoO<sub>2</sub> phase remain unaltered. The relative intensities of peaks change, but this may be due to varying levels of preferential orientation introduced during preparation of the XRD samples. In the cycled cathode, peaks due to the graphite component and an increased background due to the carbon black phase are seen (Fig. 6). Thus, bulk X-ray diffraction shows little apparent change in the structure of the LiCoO<sub>2</sub> phase upon cycling.

Electron diffraction revealed very different results. A single-crystal electron diffraction pattern from a relatively undamaged LiCoO<sub>2</sub> particle in the cycled cathode is shown in Fig. 7a. This pattern, recorded along the [0001] zone axis, is nearly identical to that of the as-calcined powder (Fig. 1b). The major spots correspond to the {11 $\bar{2}$ 0} reflections and their multiples. These are the only reflections expected for perfectly ordered HT-LiCoO<sub>2</sub>. However, the cycled particle shows weak new reflections, as indicated by the arrow. These reflections, indexed as {10 $\bar{1}$ 0}, are forbidden reflections for HT-LiCoO<sub>2</sub>. We occasionally saw these reflections in as-fired powders calcined at lower temperatures as well (e.g., 400-500°C).

A second set of new reflections was seen in highly strained particles. The SAD pattern of the severely strained LiCoO<sub>2</sub> particle in Fig. 5 is shown in Fig. 7b. These are representative of the highly strained particles which were examined in this study. The particle clearly remains single crystalline after electrochemical cycling, but

new reflections are observed between the central beam and the  $\{11\bar{2}0\}$  reflections. The weak  $\{10\bar{1}0\}$  reflections observed in the lightly strained particles and their multiples still exist but are faint, as indicated by the arrow in Fig. 7b.

The appearance of both of these new sets of reflections can be understood from the modeled structures that are listed in Table I. The cation positions are grouped into two categories: (i) varying octahedral site occupancy and (ii) tetrahedral site occupancy. In each grouping, the cation ordering has been varied within the rhombohedral  $R\bar{3}m$  space group as well as its cubic  $Fd\bar{3}m$  counterpart. Both single-crystal SAD and powder X-ray diffraction (for a random particle orientation) have been computed for each structure. Figures 8a and b show results for perfectly ordered  $\text{LiCoO}_2$  and disordered structures with varying degrees of Li-Co exchange between the octahedral site layers (models 1-3 in Table I). For the as-fired powders, the experimental XRD pattern (Fig. 1a) and the SAD pattern

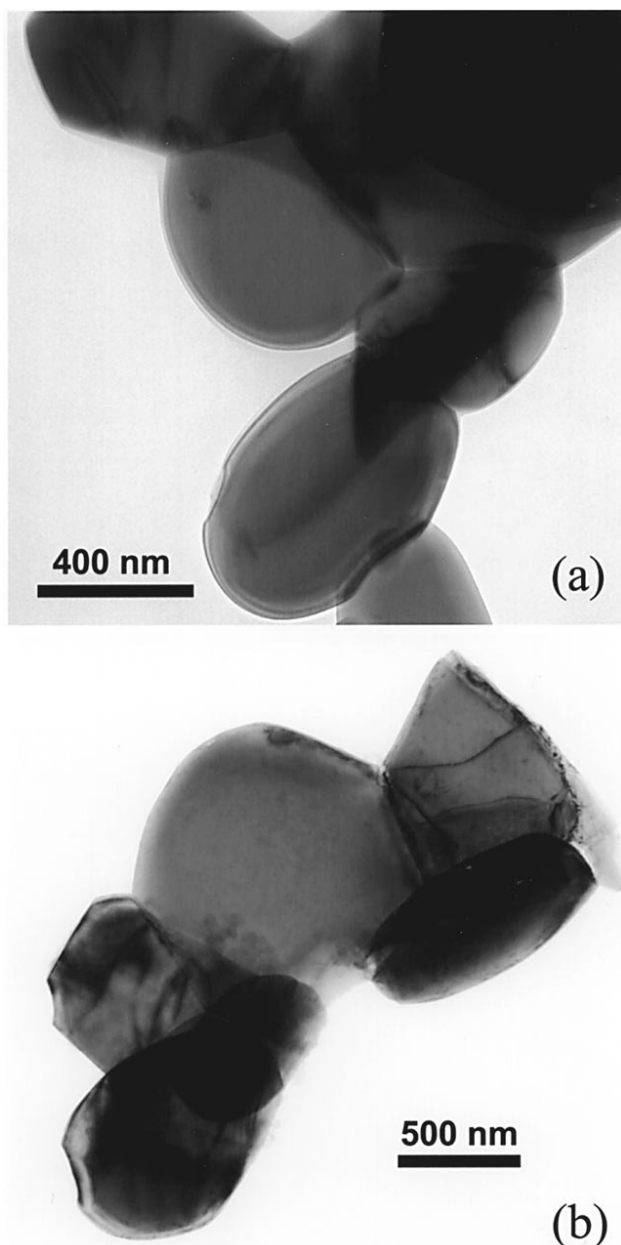


**Figure 3.** TEM bright-field image of (a) as-fired  $\text{LiCoO}_2$  powder; (b)  $\text{LiCoO}_2$  powder extracted from an electrochemical cell after cycling 50 times between 2.5 and 4.35 V. The cycled powder exhibits internal strain and dislocation defects.

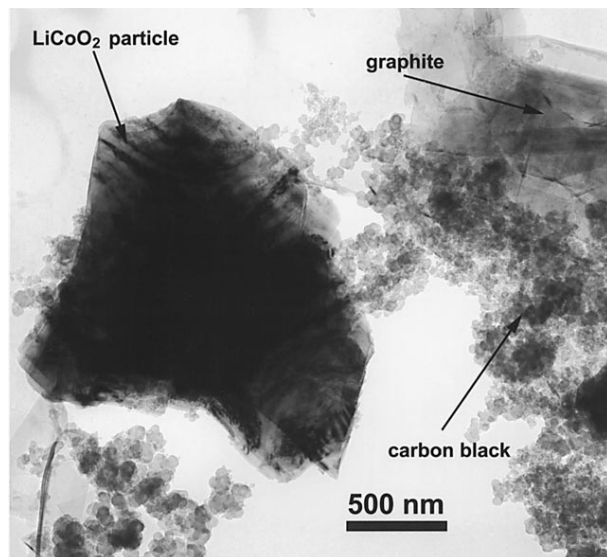


**Figure 4.** Microstructure of cathode materials after electrochemical cycling; TEM bright-field image.

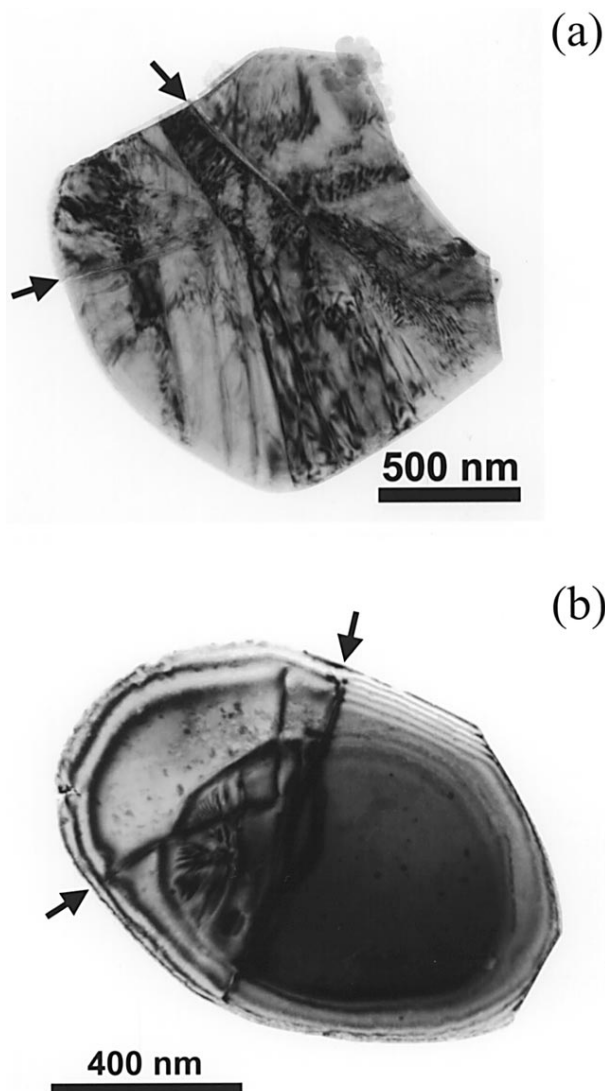


**Figure 5.** Severely damaged  $\text{LiCoO}_2$  particles from a cycled cathode showing microfracture (arrows) and strong diffraction contrast from internal strain and extended defects.

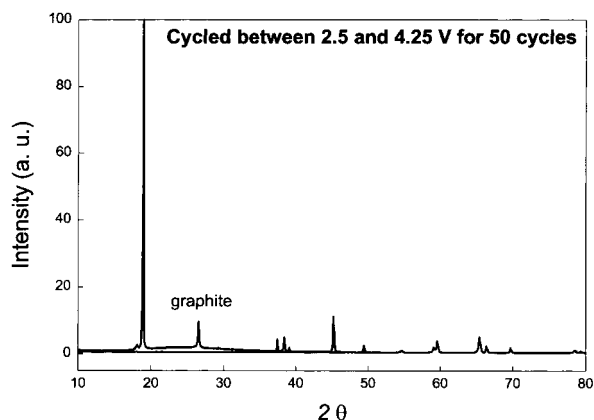


**Figure 6.** Experimental X-ray diffractogram of a composite cathode electrochemically cycled 50 times between 2.5 and 4.35 V. An increased background due to the amorphous carbon black in the cathode is seen, as well as diffraction peaks from the added graphite phase.

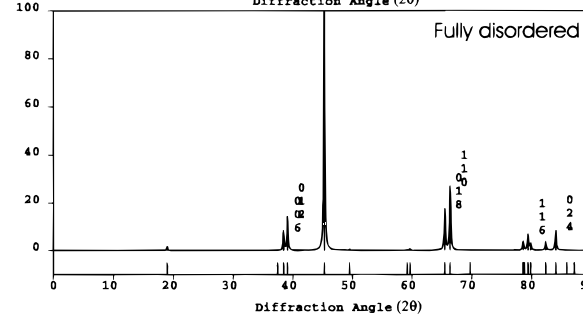
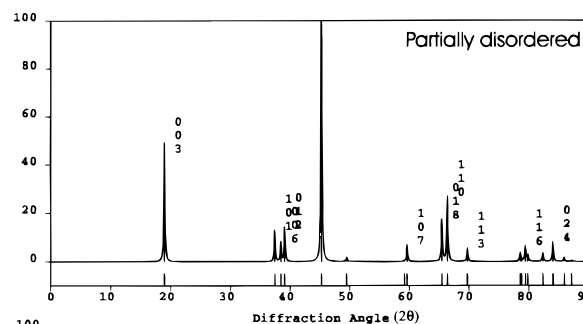
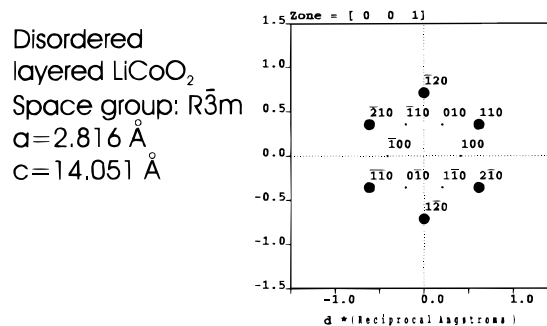
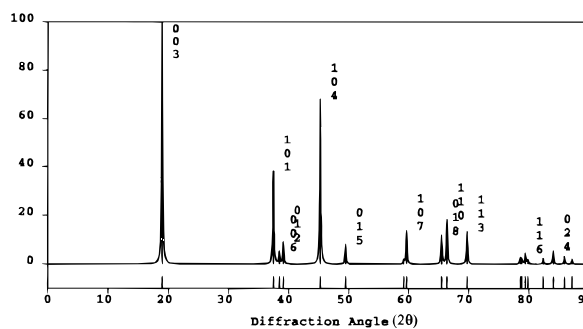
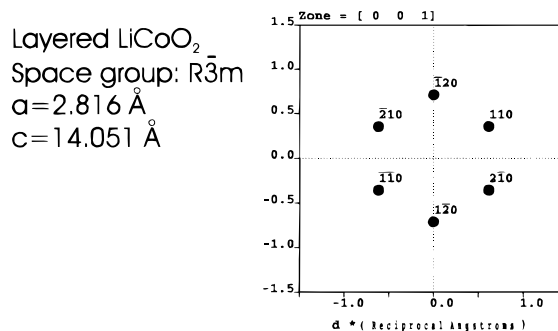


**Figure 8.** Simulated SAD and X-ray diffractograms for (a, top) perfectly ordered  $\text{LiCoO}_2$  of the  $\alpha\text{-NaFeO}_2$  structure type (space group  $R\bar{3}m$ ), corresponding to model 1 in Table I; and (b, bottom)  $\text{LiCoO}_2$  with partial and complete mixing of Li and Co among the octahedral sites, corresponding to models 2 and 3 in Table I. Simulated SAD pattern resulted from randomizing the substitutional disorder within the octahedral site layer.

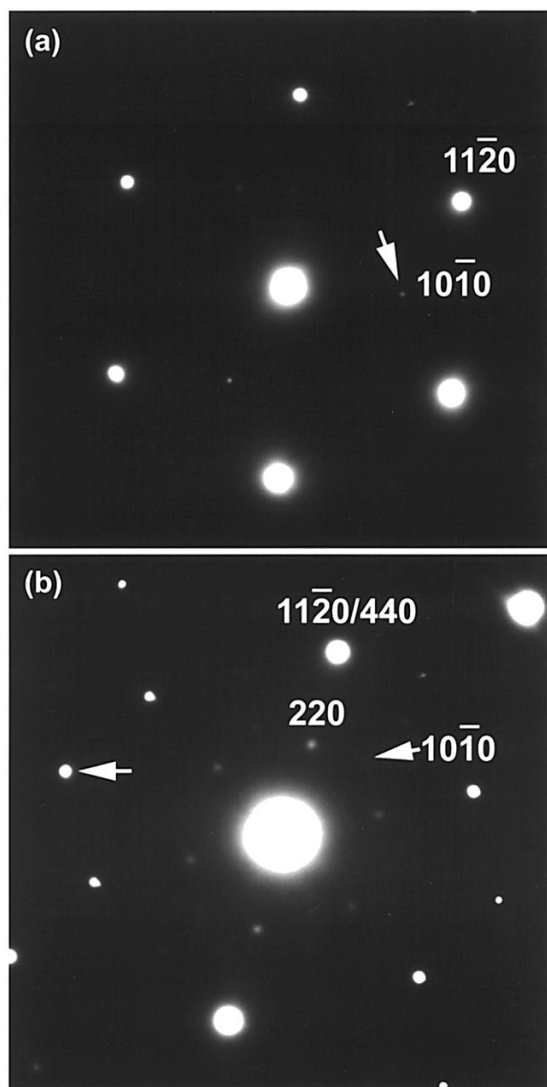


**Figure 7.** Experimental SAD patterns of cycled  $\text{LiCoO}_2$  particles. (a) A particle with low strain, indexed according to the hexagonal setting of the  $R\bar{3}m$  space group, exhibits new  $\{10\bar{1}0\}$  reflections indicating mixing of Li and Co between the octahedral sites (see text). (b) Severely strained particles exhibit a new family of reflections as well as those in (a). Indexed in the cubic setting, the new reflections correspond to spinel disorder in which cations occupy ordered 8a tetrahedral sites.

(Fig. 1b) correspond well with the simulated results for perfectly ordered HT-LiCoO<sub>2</sub> (Fig. 8a) showing that the starting material is well ordered.

**Defects on cation octahedral site layers.**—The calculation of structure factor for the ordered layered structure shows that the {10 $\bar{1}$ 0} reflections are extinct as long as the cation site symmetry is unchanged and all cations within each a and b layer have identical properties. While this can be modeled artificially using the “mixed element” approach, in reality it can occur only if a layers and b layers are each occupied by only one type of cation. Instead, when Li/Co substitutional disorder occurs, the cation sites are chemically inhomogeneous and the cation site symmetry is reduced. The structure factor for the {10 $\bar{1}$ 0} reflections becomes nonzero (Fig. 8b SAD pattern). Therefore, two types of crystallographic defects can cause the {10 $\bar{1}$ 0} reflections to be present. One is Li-Co exchange between the neighboring octahedral layers. If present, this apparently occurs without ordering within octahedral layers, because no superstructure reflections were observed experimentally in either the single-crystal SAD or powder XRD patterns of cycled materials. The simulated powder XRD pattern for this type of disorder is shown in Fig. 8b. Relative peak intensities change dramatically with disorder, with the {003} intensity diminishing greatly as cation disorder increases (models 2 and 3 in Table I). These results are consistent with previous studies that have interpreted the intensity of {003} peaks as a measure of the extent of cation mixing between octahedral layers.<sup>7</sup> However, unlike the SAD patterns, no new peaks arise in the XRD pattern due to this disorder.

The second type of disorder that can give rise to {10 $\bar{1}$ 0} reflections is cation nonstoichiometry (deficiency) within octahedral layers. Here also, if present, the vacancies appear to be randomized within the layers, because experimentally we do not see the superlattice reflections that in-plane vacancy ordering would yield.<sup>20-21</sup> Other possible reasons for the appearance of forbidden reflections are multiple diffraction events and phase separation. These are ruled out easily in the present case because only single-crystalline particles were selected for the experimental SAD patterns.

The in-plane Li/vacancy ordering studied by Delmas et al.<sup>20</sup> on delithiated LiNiO<sub>2</sub> and van der Ven et al.<sup>21</sup> on delithiated LiCoO<sub>2</sub> would give rise to superstructures that were not found in SAD for any of the single-crystal particles studied. The stage ordering described by van der Ven<sup>21</sup> also does not apply as the LiCoO<sub>2</sub> in this study is nearly fully lithiated. Therefore, we conclude that the appearance of the {10 $\bar{1}$ 0} reflections in the cycled powder is due to either random cation mixing between their respective octahedral layers, and/or cation vacancies in either layer. Of these, the presence of some Li deficiency in the discharged particles appears to be the most likely.

We ruled out the structure that has been described as “lithiated spinel”<sup>22</sup> or “modified spinel”,<sup>5</sup> obtained by electrochemical or chemical lithiation of a LiB<sub>2</sub>O<sub>4</sub> spinel compound (where B is a metal) to a Li<sub>2</sub>B<sub>2</sub>O<sub>4</sub> stoichiometry.<sup>23,24</sup> It has been proposed as a structure for LT-LiCoO<sub>2</sub>.<sup>5-9</sup> No tetrahedral sites are occupied in this structure; instead, the Co<sup>3+</sup> ions occupy 16d sites as they would in a normal spinel, whereas the Li<sup>+</sup> ions (initially on 8a tetrahedral sites) move collectively to the 16c octahedral sites upon lithiation. Model 4 in Table I represents this structure in a cubic symmetry (space group Fd $\bar{3}$ m) for Li<sub>2</sub>Co<sub>2</sub>O<sub>4</sub>, isostructural with Li<sub>2</sub>Ti<sub>2</sub>O<sub>4</sub>.<sup>24</sup> The tetragonal spinel Li<sub>2</sub>Mn<sub>2</sub>O<sub>4</sub> has the same cation ordering.<sup>23</sup> The structure can be viewed from the perspective of  $\alpha$ -NaFeO<sub>2</sub> in that the {111} planes of octahedral sites contain both Co and Li, alternating in a 3:1 and 1:3 ratio. As shown in Fig. 9a, the [111] SAD pattern of this structure is identical in symmetry to the [0001] pattern for the R $\bar{3}$ m phase of layered LiCoO<sub>2</sub>, except that the reflections are indexed as {440} in the cubic setting. Models 5 and 6 introduce increasing degrees of cation disordering into this structure via the exchange of Li and Co ions between the 16c and 16d sites (Fig. 9b). Note that although some reflections are lost upon disorder (i.e., to a disordered rock salt solid solution), unlike the rhombohedral phase no new SAD reflections appear. This is also true when cation nonstoichiometry is introduced on the 16c and 16d sites (results not

shown). Therefore, neither ordered nor disordered “lithiated spinel” can explain the SAD results in Fig. 7. In addition, we can conclude from this modeling that any particles exhibiting the {10 $\bar{1}$ 0} type reflections are rhombohedral and not cubic.

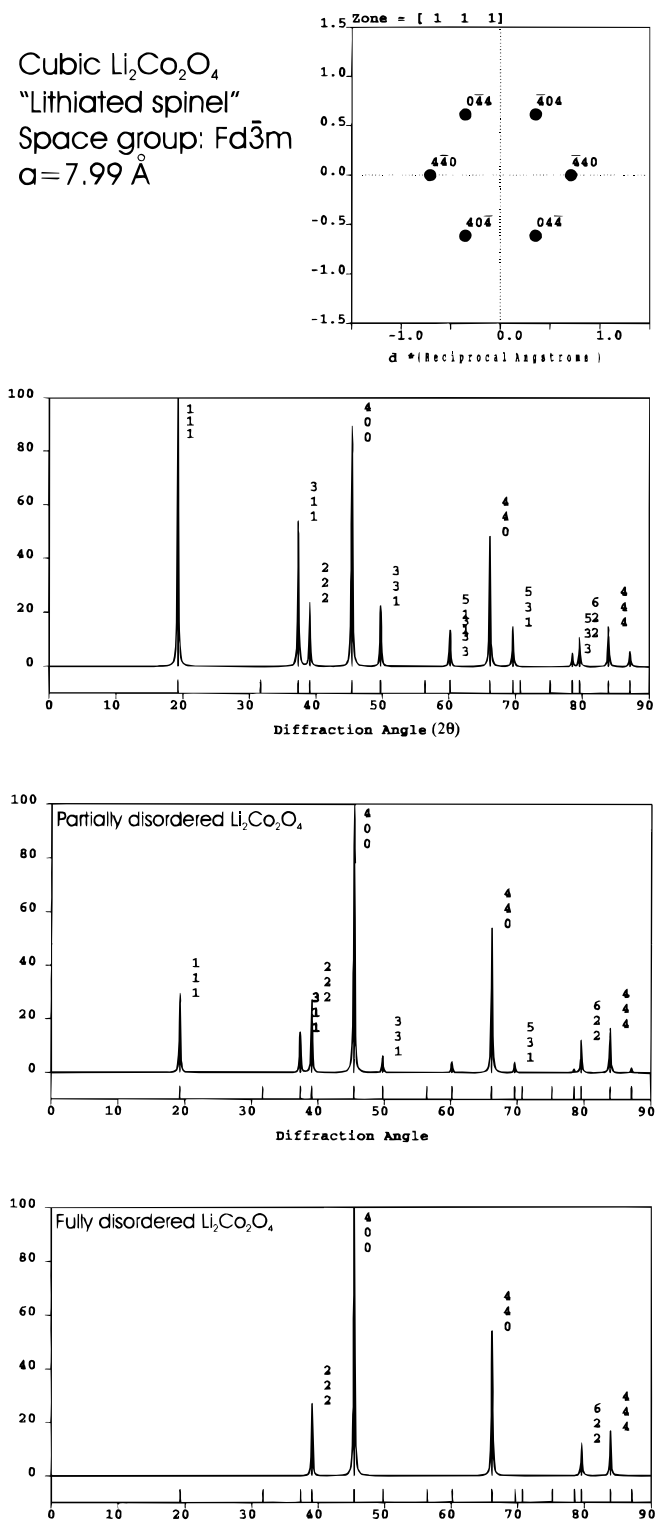


**Figure 9.** (a, top) Simulated SAD and XRD pattern of “lithiated spinel” LiCoO<sub>2</sub> with Fd $\bar{3}$ m space group in which only octahedral sites are filled (model 4). (b, bottom) Calculated XRD of this structure with partial (model 5) and complete (model 6) cation mixing between the Li and Co octahedral layers. The SAD of these structures are similar to that in (a), and do not explain either of the new sets of reflections seen experimentally in Fig. 7b.

**Tetrahedral site occupancy.**—The new reflections seen in the severely strained particles (Fig. 7b) appear only when cations occupy the ordered 8a or 8b tetrahedral sites in the  $Fd\bar{3}m$  space group; in the cubic setting they are indexed as  $\{220\}$  reflections (Fig. 10). The appearance of these reflections is easily understood by viewing a model of the spinel structure along the  $\{440\}$  planes. The ordered 8a or 8b tetrahedral sites lie in every other  $\{440\}$  plane, thereby giving rise to the  $\{220\}$  reflections (at half the  $\{440\}$  distance in reciprocal space) when they are preferentially occupied. In the ideal ordered spinel, the 8a sites are fully occupied and the 8b sites are unoccu-

pled. Although the occupancy of either gives rise to  $\{220\}$  reflections, the essential points can be made focusing on the 8a sites.

The intensity of  $\{220\}$  reflections is a function of both the tetrahedral site occupancy and the overall Li stoichiometry. Model 7 in Table I assumes a fully lithiated compound of composition  $\text{Li}_2\text{Co}_2\text{O}_4$ , in which 50% of the 8a sites are occupied by Li ions, the remainder occupying 75% of the available 16c sites. Model 8 has 100% of the 8a sites occupied by Li, leaving 50% of the 16c sites occupied by Li. The corresponding SAD patterns in Fig. 10a and b show that increasing Li occupancy on the 8a tetrahedral sites increases the intensity of

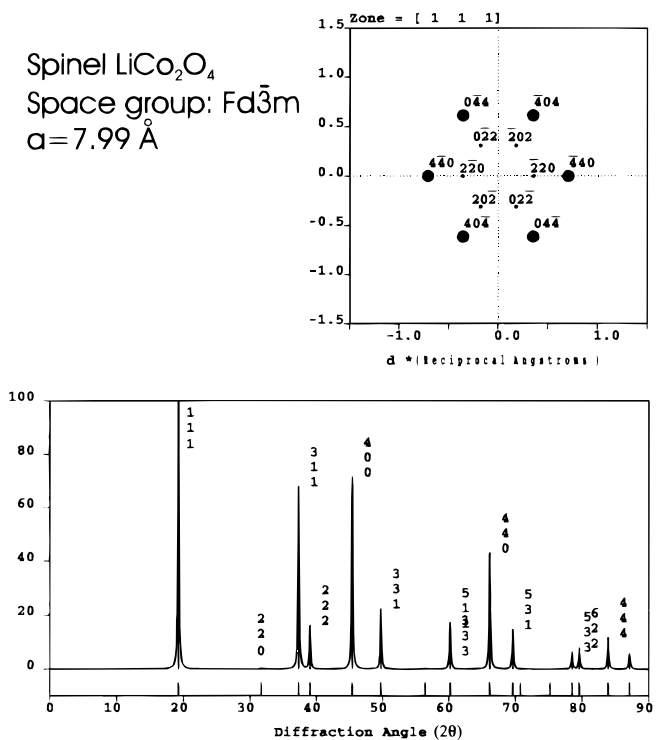
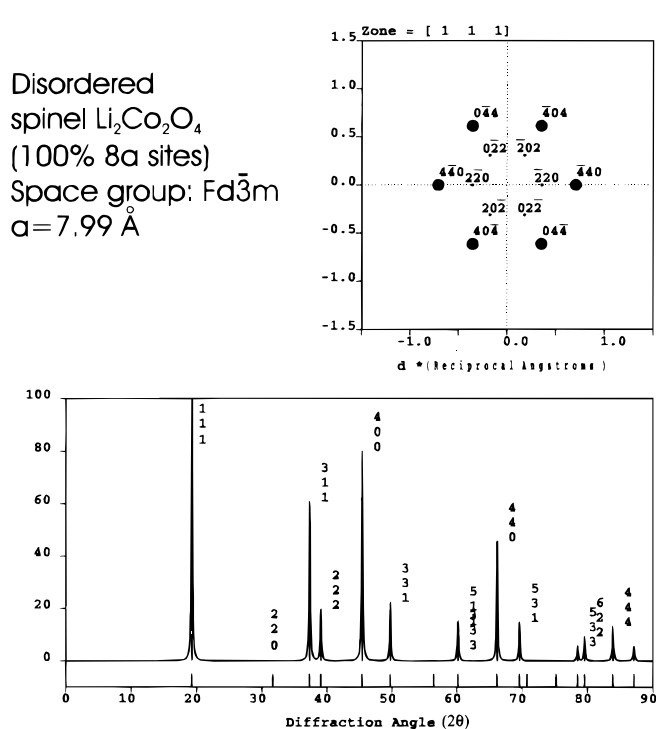
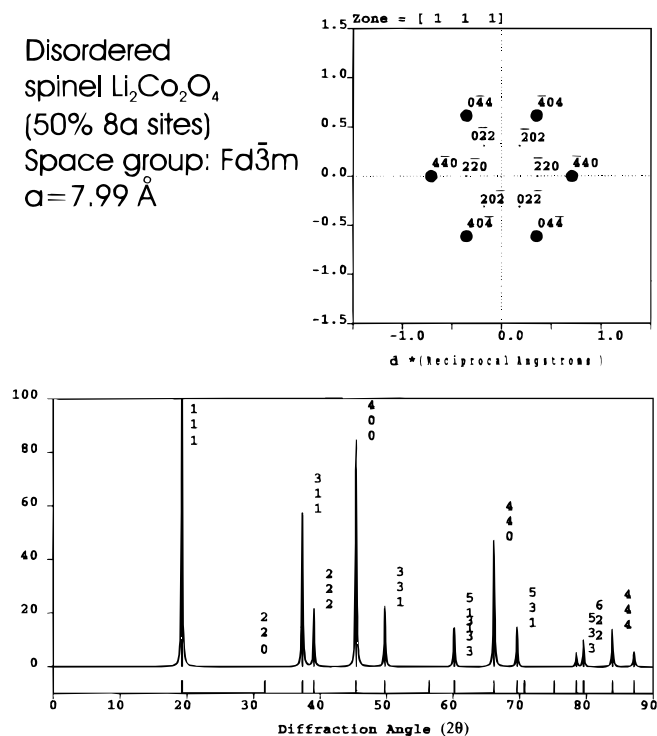


**Figure 10.** Simulated SAD and XRD patterns of (a, top left) disordered  $\text{Li}_2\text{Co}_2\text{O}_4$  spinel with 25% Li on ordered 8a tetrahedral sites (model 7), (b, above) disordered  $\text{Li}_2\text{Co}_2\text{O}_4$  spinel with one half of the Li occupying the ordered 8a tetrahedral sites, and the rest in the 16c octahedral sites (model 8), and (c, left)  $\text{LiCo}_2\text{O}_4$  of the normal spinel structure with all Li occupying ordered 8a tetrahedral sites (model 9).

the {220} reflections. Model 9 represents  $\text{LiCo}_2\text{O}_4$  of the normal spinel structure, it has the 8a sites fully occupied by Li, and no Li on the 16c sites. The corresponding SAD pattern in Fig. 10c shows that this arrangement gives the brightest {220} reflections. On the other hand, random occupation of the tetrahedral sites available in the cubic close-packed oxygen sublattice does not give rise to any {220} reflections. This is represented by model 10, a somewhat unrealistic structure in which the 16d sites are fully occupied by Co and all of the tetrahedral sites are occupied at random by Li (it is not expected to occur because simultaneous occupancy of neighboring octahedral and tetrahedral sites is required).

Notice from Fig. 10c that the {220} reflections are weak ( $\sim 1/50$ th the intensity of the {440} spots) even in perfectly ordered normal spinel  $\text{LiCo}_2\text{O}_4$ . Assuming that the highly strained particles have a nearly fully lithiated composition, as is indicated by discharging the cell to 2.5 V, we estimate from the relative intensities of the reflections in Fig. 7b that about 50% of the 8a sites are occupied by Li. The symmetry of this disordered material is still rhombohedral, as the  $\{10\bar{1}0\}$  reflections are forbidden in a cubic structure. Due to the low intensity of the {220} reflection, this form of spinel disorder is very difficult to detect by X-ray diffraction. The simulated XRD patterns for spinel disorder models 7-9, shown in Fig. 10, are indistinguishable from that of the lithiated spinel  $\text{Li}_2\text{Co}_2\text{O}_4$  with only octahedral site occupancy (model 4, Fig. 9a) until a high degree of spinel ordering is present (Fig. 10c).

**Relation to LT-LiCoO<sub>2</sub>.**—Because LT-LiCoO<sub>2</sub> has been regarded as a disordered form of HT-LiCoO<sub>2</sub>, it is of interest to compare the present electrochemically cycled materials to LT-LiCoO<sub>2</sub>.<sup>5-10</sup> Rossen et al.<sup>6</sup> showed that the layered rock salt and lithiated spinel models cannot be distinguished by X-ray and neutron diffraction, and used the difference in electrochemical properties (primarily a lower average intercalation voltage of about 3.6 V) to conclude that the lithiated spinel model applies. Gummow et al.<sup>7-9</sup> conducted both X-ray and neutron diffraction Reitveld refinements, and also concluded that fully lithiated LT-LiCoO<sub>2</sub> does not have significant tetrahedral site occupancy, proposing a model intermediate between the layered rock salt and lithiated spinel cases. Only for chemically delithiated LT-Li<sub>0.4</sub>CoO<sub>2</sub> has a spinel model with tetrahedral 8a cations<sup>9</sup> been adopted; however, it was also stressed that the material does not necessarily represent electrochemically delithiated LT-LiCoO<sub>2</sub>. A hallmark of LT-LiCoO<sub>2</sub> is also a lower and flatter intercalation voltage profile<sup>9-12</sup> compared to HT-LiCoO<sub>2</sub>. The flat voltage plateau indicates a two-phase region, which Gummow et al.<sup>8</sup> suggest is the coexistence of  $\text{Li}_2\text{Co}_2\text{O}_4$  lithiated spinel and  $\text{LiCo}_2\text{O}_4$  normal spinel.

As we have shown, electrochemically cycled  $\text{LiCoO}_2$  does not have the lithiated spinel structure, does not have tetrahedral site occupancy, and does not exhibit a lower and flatter intercalation voltage. Therefore it bears little similarities to LT-LiCoO<sub>2</sub>. The appearance of tetrahedral site spinel disorder is particularly significant. Whereas the spinel is widely believed to be the most stable phase of lithium manganese oxides, and both the monoclinic and orthorhombic polymorphs of  $\text{LiMnO}_2$  are observed to transform to the spinel upon cycling,<sup>25-32</sup> this has not previously been thought to be the case in  $\text{LiCoO}_2$ . Concurrently with this study, van der Ven and Ceder<sup>33</sup> have found through ab initio modeling that spinel is the ground state for delithiated  $\text{LiCoO}_2$  (e.g.,  $\text{LiCo}_2\text{O}_4$ ). This is in accordance with the present finding that HT-LiCoO<sub>2</sub> can transform to the spinel structure during electrochemical cycling.

Even though the present cathodes are electrochemically quite stable to 50 cycles, TEM results show that, locally, microstructural and crystallographic change has already occurred. Accumulated damage of this kind may therefore be responsible for degradation in  $\text{LiCoO}_2$ -based batteries upon overcharging or after extended cycling.

### Conclusions

Electrochemical cycling creates a variety of defects in the  $\text{LiCoO}_2$  particles in a typical composite cathode. Although by bulk X-ray diffraction analysis the oxide phase appears unchanged, direct

TEM examination shows that a significant fraction of the particles are severely strained, fractured, and contain a high density of extended defects. The extent of damage varies widely among  $\text{LiCoO}_2$  particles in the same cathode. Selected-area diffraction shows that cycled particles exhibit two types of new reflections. One arises from exchange of Li and Co between their respective octahedral site layers, and/or cation deficiency, most likely in the Li layers. The second set of new reflections, seen in the more severely strained particles, demonstrates unequivocally the presence of spinel ordering whereby tetrahedral spinel sites are occupied by Li. This disorder is not detectable by bulk X-ray diffraction techniques, and represents the first direct evidence for cycling-induced spinel disorder in HT-LiCoO<sub>2</sub>.

### Acknowledgments

We would like to thank G. Ceder and A. van der Ven for fruitful discussions. This work has been funded by the INEEL University Research Consortium. The INEEL is managed by Lockheed Martin Idaho Technology Company for the U.S. Department of Energy, Idaho Operations Office, under contract no. DE-AC07-94ID13223. We also used the instrumentation in the Shared Central Facilities in the Center for Materials Science and Engineering at MIT, supported by NSF grant no. 9400334-DMR.

Massachusetts Institute of Technology assisted in meeting the publication costs of this article.

### References

- W. D. Johnston, R. R. Heikes, and D. Sestrich, *J. Phys. Chem. Solids*, **7**, 1 (1958).
- K. Mizushima, P. C. Jones, P. J. Wiseman, and J. B. Goodenough, *Mater. Res. Bull.*, **15**, 783 (1980).
- H. J. Orman and P. J. Wiseman, *Acta Crystallogr.*, **C40**, 12 (1984).
- T. A. Hewston and B. L. Chamberland, *J. Phys. Chem. Solids*, **48**, 97 (1987).
- J. N. Reimers, W. Li, E. Rossen, and J. R. Dahn, *Mater. Res. Soc. Symp. Proc.*, **293**, 3 (1993).
- E. Rossen, J. N. Reimers, and J. R. Dahn, *Solid State Ionics*, **62**, 53 (1993).
- R. J. Gummow, M. M. Thackeray, W. I. F. David, and S. Hull, *Mater. Res. Bull.*, **27**, 327 (1992).
- R. J. Gummow, D. C. Liles, and M. M. Thackeray, *Mater. Res. Bull.*, **28**, 235 (1993).
- R. J. Gummow, D. C. Liles, M. M. Thackeray, and W. I. F. David, *Mater. Res. Bull.*, **28**, 1177 (1993).
- B. Garcia, P. Barboux, F. Ribot, A. Kahn-Harari, L. Mazerolles, and N. Baffier, *Solid State Ionics*, **80**, 111 (1995).
- G. G. Amatucci, J. M. Tarascon, and L. C. Klein, *Solid State Ionics*, **84**, 169 (1996).
- Y.-M. Chiang, Y.-I. Jang, H. Wang, B. Huang, D. R. Sadoway, and P. Ye, *J. Electrochem. Soc.*, **145**, 887 (1998).
- J. N. Reimers and J. R. Dahn, *J. Electrochem. Soc.*, **139**, 8 (1992).
- G. G. Amatucci, J. M. Tarascon, and L. C. Klein, *J. Electrochem. Soc.*, **143**, 3 (1996).
- T. Ohzuku and A. Ueda, *J. Electrochem. Soc.*, **141**, 2972 (1994).
- T. Ohzuku, A. Ueda, N. Nagayama, Y. Iwakoshi, and H. Komori, *Electrochim. Acta*, **38**, 1159 (1993).
- T. Ohzuku, H. Tomura, and K. Sawai, *J. Electrochem. Soc.*, **144**, 3496 (1997).
- B. Huang, Y.-I. Jang, Y.-M. Chiang, and D. R. Sadoway, *J. Appl. Electrochem.*, in press (1998).
- J. W. Edington, *Practical Electron Microscopy in Materials Science*, Van Nostrand Reinhold, New York (1976).
- C. Delmas, J. P. Peres, A. Rougier, A. Demourgues, F. Weill, A. Chadwick, M. Broussely, F. Pertont, Ph. Biensan, and P. Willmann, *J. Power Sources*, **68**, 120 (1997).
- A. van der Ven, M. K. Aydinol, and G. Ceder, *Phys. Rev. B*, **58**, 2975 (1998).
- M. M. Thackeray, *Prog. Solid State Chem.*, **25**, Elsevier Publishers, Amsterdam (1997).
- J. M. Tarascon and D. Guyomard, *J. Electrochem. Soc.*, **138**, 2864 (1991).
- R. J. Cava, D. W. Murphy, S. Zahurak, A. Santoro, and R. S. Roth, *J. Solid State Chem.*, **53**, 64 (1984).
- R. J. Gummow and M. M. Thackeray, *J. Electrochem. Soc.*, **141**, 1178 (1994).
- J. N. Reimers, E. W. Fuller, E. Rossen, and J. R. Dahn, *J. Electrochem. Soc.*, **14**, 3396 (1993).
- R. J. Gummow, D. C. Liles, and M. M. Thackeray, *Mater. Res. Bull.*, **28**, 1249 (1993).
- I. J. Davidson, R. S. McMillan, J. J. Murray, and J. E. Greedan, *J. Power Source*, **54**, 232 (1995).
- I. Koetschau, M. N. Richard, J. R. Dahn, J. B. Soupart, and J. C. Rousche, *J. Electrochem. Soc.*, **142**, 2906 (1995).
- L. Croguennec, P. Deniard, R. Brec, P. Biensan, and M. Broussely, *Solid State Ionics*, **89**, 127 (1996).
- L. Croguennec, P. Deniard, and R. Brec, *J. Electrochem. Soc.*, **144**, 3323 (1997).
- G. Vitins and K. West, *J. Electrochem. Soc.*, **144**, 2587 (1997).
- A. van der Ven and G. Ceder, Private communication.